THE JOURNAL OF PHYSICAL CHEMISTRY Letters

Letter

pubs.acs.org/JPCL

Covalent Linking Greatly Enhances Photoinduced Electron Transfer in Fullerene-Quantum Dot Nanocomposites: Time-Domain Ab Initio Study

Vitaly V. Chaban,[†,‡] Victor V. Prezhdo,[§] and Oleg V. Prezhdo*[,†]

[†]Department of Chemistry, University of Rochester, Rochester, New York 14627, United States

[‡]MEMPHYS − Center for Biomembrane Physics, Odense M. 5230, Denmark

[§]Institute of Chemistry, Jan Kochanowski University, 25-406 Kielce, Poland

ABSTRACT: Nonadiabatic molecular dynamics combined with time-domain density functional theory are used to study electron transfer (ET) from a CdSe quantum dot (QD) to the C_{60} fullerene, occurring in several types of hybrid organic/inorganic nanocomposites. By unveiling the time dependence of the ET process, we show that covalent bonding between the QD and C_{60} is particularly important to ensure ultrafast transmission of the excited electron from the QD photon-harvester to the C_{60} electron acceptor. Despite the close proximity of the donor and acceptor species provided by direct van der Waals contact, it leads to a notably weaker QD-C_{60} interaction than a lengthy molecular bridge. We show that the ET rate in a nonbonded mixture of QDs and C_{60} can be enhanced by doping. The photoinduced ET is promoted primarily by mid- and low-frequency vibrations. The study establishes the basic design principles for enhancing photoinduced charge separation in nanoscale light harvesting materials.

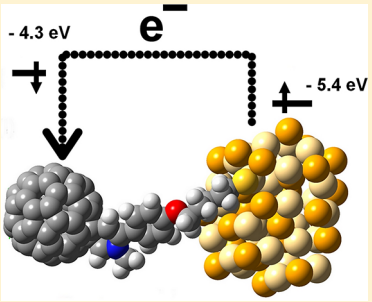

SECTION: Energy Conversion and Storage; Energy and Charge Transport

A great variety of solar cell designs are proposed and investigated worldwide.[1−6] Photosynthetic membranes, conjugated polymers, sensitizer chromophores, inorganic semiconductors, and other materials serve as light-harvesting antennas in liquid-junction,[7] hybrid organic,[8] thin film,[9] and other types of photovoltaic and photocatalytic devices. Utilization of nanoscale architectures in light energy conversion into electrical and chemical energy has emerged as an alternative to single-crystalline devices. Low material cost, easy methods of fabrication, high light absorption cross sections, and ability to tune continuously the optical response make inorganic semiconductor nanocrystals attractive candidates for photon harvesting.[7,10−12] To achieve photoinduced charge separation, nanocrystals can be coupled to wide band gap inorganic semiconductors, such as titanium and zinc oxides,[13−15] replacing molecular chromophore in dye-sensitized semiconductor solar cells.[2,4,16] Nanoscale carbon, including graphene,[17] carbon nanotubes,[18] and fullerenes,[19] represents another class of materials that are actively explored for solar energy applications. Hybrid organic/inorganic composites, combining nanoscale carbon with semiconductor quantum dots (QDs), are synthetized and tested for light-energy-harvesting purposes.

Recently, a number of groups have produced and characterized experimentally hybrid inorganic/organic QD/fullerene nanocomposites for solar energy applications.[19−25] A variety of architectures are being explored, including both mechanical mixtures of fullerenes and QDs[20−23,25] and covalently linked composites.[19,24] Bang and Kamat[19] reported utilization of fullerenes in QD solar cells by placing a blend of CdSe QDs and C_{60} on an optically transparent electrode using electrophoretic deposition. By functionalizing C_{60} with a thiol compound, they linked it covalently to the QD and investigated the photoinduced electron transfer (ET) from the QD to C_{60} using time-resolved transient absorption spectroscopy. The covalent linking provided a significant improvement in the charge separation and photoconversion efficiency compared with the previous work utilizing a mechanical blend.[20]

The current letter reports state-of-the-art time-domain ab initio simulations of the photoinduced ET in a series of fullerene−CdSe QD nanocomposites, including both covalently linked and mechanically mixed compounds. Directly mimicking the recent experimental work of Kamat and coworkers[19] in real time and at the atomistic level, the study provides detailed insight into the charge-separation processes in the novel nanoscale composite material. Good agreement with the experimental data is achieved. The simulations show that both binding energy and electronic donor−acceptor coupling between the two species are much weaker in the mechanical mixture, despite the significantly shorter distance between the QD and C_{60} relative to the covalently linked couple. The noncovalent interaction and ET rate between the QD and C_{60} is enhanced by doping the latter with Li. The study characterizes the vibrational modes that promote the photo-

Received: November 17, 2012
Accepted: December 10, 2012
Published: December 10, 2012

induced ET and accommodate the excess electronic energy and generally provides important design principles for achieving efficient charge separation in hybrid organic/inorganic composites.

The simulations utilize the quantum-classical fewest-switches surface-hopping technique[26] implemented within the time-dependent Kohn−Sham scheme[27,28] and including the semiclassical correction for quantum decoherence.[29] The decoherence times were computed using the optical response formalism, as described, for instance, in refs 30 and 31. The method has been previously applied to study ET and relaxation dynamics at interfaces of inorganic semiconductors with molecular chromophores,[16] QDs,[32] and graphene,[33] in carbon nanotubes,[29] nanoribbons,[34] semiconducting,[35] and metallic[36] nanocrystals and in biological systems.[27]

The approach provides a detailed ab initio picture of the coupled electron-vibrational dynamics on the atomic scale and in the time-domain. After an initial excitation, the simulated system is allowed to evolve in the electronic state manifold coupled to semiclassical phonons. Nonadiabatic couplings, computed on the fly, induce electronic transitions. A detailed description of the method can be found elsewhere.[27,29,37]

The electronic structure of the QD-C_{60} hybrid was obtained using a converged plane-wave basis and the Perdew, Burke, and Ernzerhof (PBE)[38] density functional. The inner electron shells were represented with projector-augmented-wave (PAW) pseudopotentials to reduce the computational cost of the simulations. The Vienna ab initio simulation program (VASP)[39] was employed. The energy cutoff was set to 500 eV (36.75 Ry) for all systems, as dictated by the hardest pseudopotential.[40] The geometries of the systems were optimized first, using the conjugate gradient algorithm with the absolute energy convergence threshold of 0.001 eV. Then, the systems were heated from 0 to 300 K during 5.0 ps using uniform velocity rescaling. Finally, trajectories for nonadiabatic electron-vibrational dynamics were generated in the constant energy ensemble. The nonadiabatic trajectories were 2.0 ps long for system (I), which showed faster ET, and 6.0 ps for systems (II) and (III). The nuclear time step for the equilibration and production runs was set to 1.0 fs. The electronic time step for nonadiabatic dynamics was 1.0 as.

Figure 1 depicts the optimized geometries of the simulated systems. Three architectures of the hybrid organic/inorganic material are considered. The first one includes the magic-size $Cd_{33}Se_{33}$ QD chemically linked to the thiol-functionalized C_{60}, as implemented in the recent experimental study.[19] The second architecture involves the $Cd_{33}Se_{33}$ QD, weakly interacting with the pristine C_{60}. This system mimics mechanical mixtures,[20−23,25] providing the simplest way to prepare such a kind of nanoscale composite. The third system contains Li-encapsulated C_{60}, which can be prepared experimentally.[41] The hybrid organic/inorganic photovoltaic material combining an alkali-doped C_{60} and a semiconductor QD is considered for the first time. The principal idea beyond the encapsulation of the alkali atom is to increase the intermolecular interaction and therefore to enhance the ET rate. The $2s^1$ valence electron of lithium is expected to localize on the carbon atoms of fullerene.[41] C_{60} attains a negative charge, which should induce stronger electrostatic interactions with the QD.

The optimized geometries of C_{60} are essentially the same for all three systems, whereas the arrangements of the $Cd_{33}Se_{33}$ atoms differ somewhat, Figure 1. In particular, the Cd atoms in system (III) are closer to the fullerene than the Se atoms,

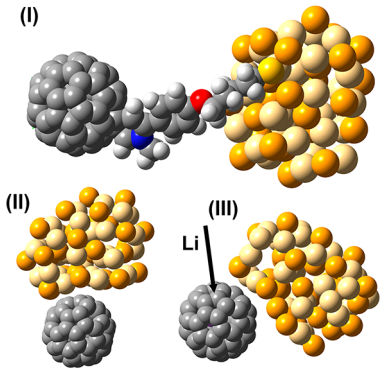

Figure 1. Optimized geometries of the simulated systems, consisting of the $Cd_{33}Se_{33}$ QD and the C_{60} fullerene. Three bonding patterns are explored: (I) covalent binding via a molecular bridge as in the experiment,[19] (II) weak nonbonded interactions, mimicking a mechanical mixture,[20] and (III) using Li-encapsulated C_{60}.[41] C is gray, N is blue, O is red, S is yellow, H is white, Cd is bright yellow, and Se is pale yellow. Whereas the presence of the Li atom inside C_{60} does not appreciably change the structure of the complex, it increases the QD-C_{60} binding energy by a factor of 2.5, Table 1.

whereas in system (II) the Cd and Se atoms approach the C_{60} surface by about the same distance. Following the Bader partition scheme, the analysis of the partial charges indicates nearly a full electron transfers from the encapsulated Li onto C_{60}, whereas no charge transfer to the QD is observed. At zero temperature, the excess charge localized on C_{60} is equal to −0.99 e, whereas Li possesses an extra +0.99 e. At 300 K in the ground electronic state, the transferred charge oscillates between 0.94 and 0.99 e. The significant amount of charge transfer between Li and C_{60} indicates ionic bonding between these particles, which is successfully captured by the PBE functional[38] and the converged plane wave basis set. The Li atom exists in the cation form, whereas fullerene, as a more electronegative species, becomes an anion. The electron charge on the QD is not perturbed by interaction with C_{60}, being on average +0.70 e on Cd and −0.70 e on Se. Interestingly, the standard deviation of the Bader charge on Se (±0.08 e) is four time higher than that on Cd (±0.02 e), at room temperature. Note that our time-dependent density functional theory (DFT) simulation treats explicitly only the 12 highest-energy electrons of each Cd atom and six electrons of each Se atom, whereas all other electrons are represented implicitly using the PAW pseudopotentials.[40]

The calculated zero-temperature energy gaps are 1.4 and 1.8 eV for the standalone QD and fullerene, respectively. Quite remarkably, the gap between the highest occupied molecular orbital (HOMO) and the lowest unoccupied molecular orbital (LUMO) of C_{60}, as well as their absolute energies relative to the vacuum level, E_{HOMO} = −6.1 eV and E_{LUMO} = −4.3 eV, reproduce the experimental values[42] of −6.2 and −4.3 eV with nearly perfect accuracy. The HOMO−LUMO gap of $Cd_{33}Se_{33}$ is underestimated[43] due to the well-known systematic errors of pure DFT functionals and excitonic effects.[44] The gap corresponds to larger diameter CdSe QDs, effectively representing the experimental system.[19] The QD HOMO−LUMO gap is slightly smaller in system (I) than systems (II) and (III), Figure 2, because the QD wave function leaks onto the bridge, effectively increasing the QD size. The presence of Li inside C_{60} breaks the degeneracy of the C_{60} LUMO. The bottom panel of Figure 2 shows the highest orbital of the

dx.doi.org/10.1021/jz301878y | J. Phys. Chem. Lett. 2013, 4, 1−6

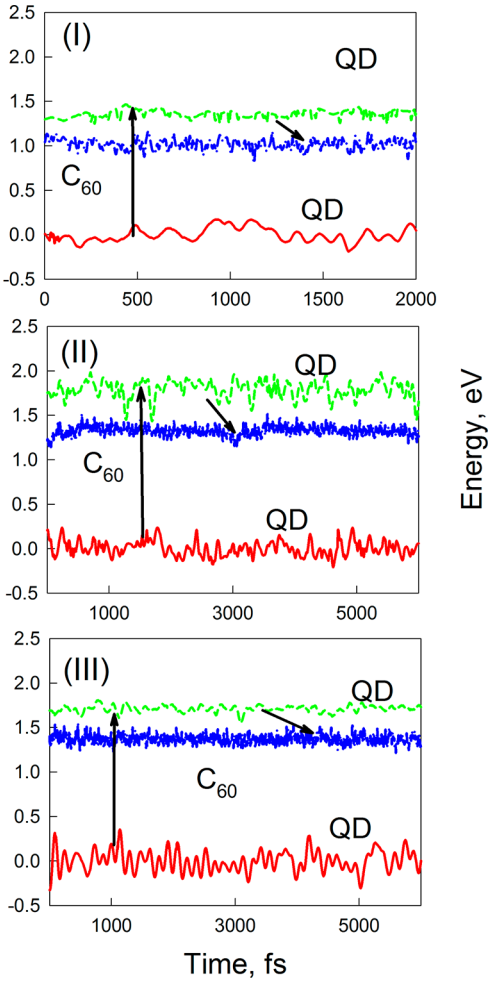

Figure 2. Evolution of the key QD and C_{60} state energies induced by vibrational motions. Panels (I), (II) and (III) correspond to the systems depicted in Figure 1. The upward and downward arrows show electron photoexcitation and subsequent transfer. The QD band gap is slightly smaller in system (I) involving a molecular bridge than in the noncovalently bound complexes (II) and (III), because the QD wave functions extend onto the bridge, effectively increasing the QD size. The average QD HOMO energy is set to zero.

LUMO manifold because it is energetically closest to the QD LUMO populated by the photoexcited electron and determines the ET rate.

The photoinduced electron−phonon dynamics in the organic/inorganic hybrid under consideration starts with an optical excitation of the QD from HOMO to LUMO, Figure 2. Then, the electron is transferred from the QD LUMO to the C_{60} LUMO, as a result of a nonadiabatic transition. The excess electronic energy is deposited into vibrational modes. In systems (II) and (III), the HOMO and LUMO densities are localized on either fullerene or $Cd_{33}Se_{33}$ and never on both particles at the same time, Figure 3. The QD HOMO in the Li-doped system presents a minor exception because it shows a small amount of density on C_{60}. In general, the presence of the Li atom inside C_{60} notably alters the densities of all states involved in the photoinduced ET process. The QD and fullerene orbitals are partially delocalized onto the molecular bridge, in system (I); however, the bridge orbitals are energetically separated from the orbitals of the QD and C_{60}. The latter fact, confirmed by the direct nonadiabatic dynamics

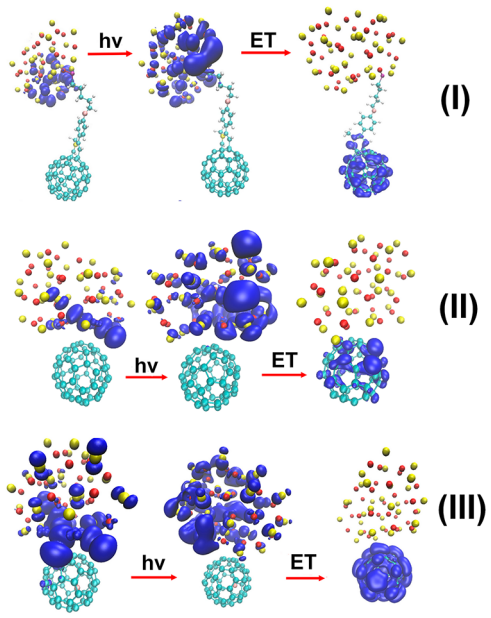

Figure 3. Densities of the molecular orbitals participating in the electron excitation and transfer processes. Left to right, the orbitals are QD HOMO, QD LUMO, and C_{60} LUMO. The orbital energies are given in Figure 2.

simulation, proves that the electron never populates the bridge during the ET process, even though the molecule provides the donor−acceptor coupling.

The energy levels of the organic/inorganic hybrid material undergo significant fluctuations due to nuclear motions at room temperature, Figure 2. At certain points along the molecular dynamics trajectory, the LUMOs of the QD and C_{60} closely approach each other, and the electronic energy gap involved in the ET process almost vanishes. The states do not cross, however, and the problems stemming from the adiabatic representation of weakly interacting systems[45] do not arise. Furthermore, because the NA couplings are evaluated numerically by computing the overlap of the DFT orbitals at different time steps,[37] the divergence of the energy denominator in the analytical evaluation of the coupling is avoided. The largest fluctuations are recorded in system (II), where the QD-C_{60} binding is weakest and the nonadiabatic ET coupling is smallest, Table 1. It is interesting to note that, on the one hand, weak interaction between the donor and acceptor species in system (II) inhibits ET, whereas on the other hand, larger energy gap fluctuations facilitate ET. The average energy

Table 1. Electron Transfer (ET) Time, Pure-Dephasing Time, Average Absolute Values of the Non-Adiabatic (NA) Coupling, and Fullerene-Quantum Dot Binding Energies for the Three Simulated Systems, Figure 1[a]

system	ET time, ps	dephasing time, fs	NA coupling, meV	binding energy, kJ mol^{-1}
I	7.66	15	2.96 (6.85)	4853
II	37.4	11	0.874 (1.29)	19.0
III	27.7	20	1.60 (2.54)	51.3

[a]ET time, dephasing time, and NA coupling are computed at 300 K; the binding energies correspond to the optimized structures. The values in parentheses give standard deviations (fluctuations) in the NA coupling.

dx.doi.org/10.1021/jz301878y | J. Phys. Chem. Lett. 2013, 4, 1−6

difference between the orbitals involved in the ET equals 0.34, 0.42, and 0.34 eV for systems (I), (II), and (III), respectively.

The energy of covalent binding in system (I) is two orders of magnitude higher than the energy of nonbonding interactions in systems (II) and (III). Li encapsulation inside C_{60} increases the QD-C_{60} binding energy by a factor of 2.5, Table 1. The encapsulation increases the nonadiabatic coupling between the electron donor and acceptor orbitals by a factor of 2. The difference between the nonadiabatic coupling for the covalently bonded and nonbonded systems is significant, but it is much smaller than the corresponding difference in the binding energies. The large fluctuation in the nonadiabatic coupling, Table 1, is closely to the oscillations in the orbital energies, Figure 2.

The dephasing times reported in Table 1 represent the lifetimes of quantum-mechanical coherences between the electron donor and acceptor orbitals during the ET process. The generation of coherences is essential for the quantum-mechanical transition. Rapid decay of coherences is indicative of strong elastic electron−phonon scattering. The nonadiabatic coupling and decoherence represent the inelastic and elastic components of the electron−vibrational interaction. The values of both nonadiabatic couplings and dephasing times, Table 1, are typical of nanoscale systems.[30,31,35] The longer dephasing observed with the covalently linked (I) and doped (III) systems, relative to the mechanical mixture (II), enhances the ET rate because rapid dephasing results in the quantum Zeno effect stopping quantum transition altogether.[46]

The ET from the QD to C_{60} occurs via a nonradiative transition between the corresponding states. The time-dependent population of the donor state illustrates the evolution of the ET process in Figure 4. Assuming that the nonradiative decay is

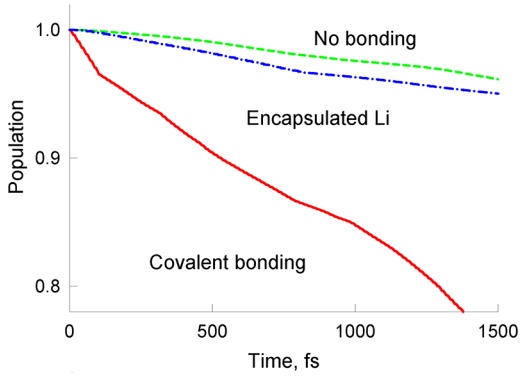

Figure 4. Electron transfer from the CdSe QD LUMO to the C_{60} LUMO, represented by the time-dependent population of the donor orbital. The time constants obtained by exponential fits of the data are given in Table 1.

exponential, as determined in the experiments,[19] the simulation data were fit using the expression $P(t) = \exp(-t/\tau) \approx 1 - t/\tau$. The ET times, τ, are reported in Table 1. By far the fastest ET (7.66 ps) occurs in system (I), where C_{60} and $Cd_{33}Se_{33}$ are connected via the covalent molecular bridge, Figure 1. The calculated ET time is in good agreement with the reported experimental values.[19] The nonadiabatic couplings are smaller in systems (II) and (III), as stipulated by the weaker nonbonding interactions, Table 1. As a result, these systems demonstrate larger ET times. ET in system (III) occurs 1.4 times faster than in system (II). This fact indicates that the encapsulated Li atom enhances the electron donor−acceptor interaction, even though the electronic states of Li are not directly involved in the ET process. This finding illustrates that C_{60} doping presents an interesting opportunity for increasing the ET rate in mechanical mixtures of QDs and fullerenes. Covalent QD-C_{60} binding remains the preferred mechanism for enhancing the charge-separation efficiencies, rationalizing the improved photoconversion efficiencies in the covalently linked systems relative to the mechanical mixtures, reported in the experiments.[19]

Vibrational motions of the organic and inorganic components involved in the ET process are responsible for the fluctuation of the energy gap between the donor and acceptor states (Figure 2), create the nonadiabatic coupling between the states (Table 1), and accommodate the excess electronic energy released during ET. To characterize the vibrational motions involved in the ET process, we computed Fourier transforms of the autocorrelation functions of the donor−acceptor energy gaps along the microcanonical ground-state trajectories. Figure 5 visualizes the resulting influence spectra for the

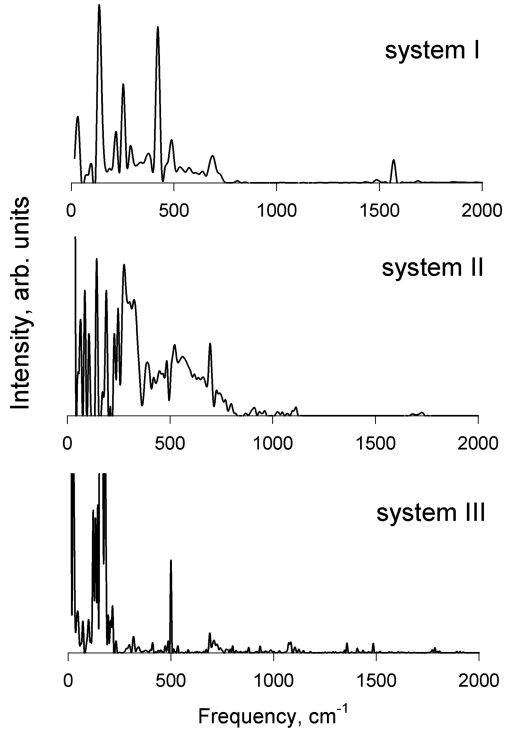

Figure 5. Phonon modes participating in the photoinduced electron transfer process in the three systems, Figure 1. The data are obtained by computing Fourier transforms of the autocorrelation functions of the fluctuation of energy gaps between the donor and acceptor states, Figure 2. The electron transfer is facilitated primarily by the polar low-frequency modes arising from the CdSe QD. The spectrum of system (I), involving a molecular bridge, shows better resolved peaks, including a signal at 1600 cm^{-1} corresponding to the C−C stretch of the bridge.

three simulated systems. All systems exhibit a variety of peaks below 1000 cm^{-1}, corresponding to vibrations of the heavy elements of the QD as well as bending and torsional motions of the C atoms of C_{60}. It is instructive to observe that the C−C stretching mode around 1600 cm^{-1} is clearly seen in system (I) but is essentially nonexistent in systems (II) and (III). The signal arises from the molecular bridge, confirming that ET in system (I) takes place through the bridge rather than through

dx.doi.org/10.1021/jz301878y | J. Phys. Chem. Lett. 2013, 4, 1−6

the empty space. Overall, the phonon modes of the QD couple to the ET process more significantly than the C_{60} vibrations, as evidenced by the notably larger fluctuations in the energy levels of $Cd_{33}Se_{33}$ than C_{60}, Figure 2. This result is rationalized by the fact that the vibrational modes of the QD are polar because the Cd and Se atoms carry positive and negative charges, respectively. Polar motions couple electrostatically to the transferred electron. In contrast, the modes of C_{60} are nonpolar and have much less influence on the ET dynamics.

By extrapolating the results of the current calculations to related systems and processes, we should note that the factors enhancing the forward ET from the QD to C_{60} can also speed up the back ET, leading to electron−hole recombination and losses in photovoltaic current. By simultaneously covalently linking C_{60} to QDs and C_{60} doping, one can enhance the ET rates further, although the combined effects are unlikely to add up in a linear way. Increasing the bridge length should lead to a weak, exponential decrease in the ET rate. Replacing CdSe with CdS should not change the forward ET dynamics because the conduction band of both semiconductors is composed of the d orbitals of Cd atoms. At the same time, the back ET rate is more likely to change because the valence bands are generated by the s and p orbitals of S atoms.

To recapitulate, we have carried out nonadiabatic molecular dynamics simulations combined with time-domain DFT, characterizing the photoinduced ET transfer from a CdSe QD to the C_{60} fullerene. For the first time, the state-of-the-art technique has been applied successfully to a noncovalently bound system. We have shown that a covalent bridge connecting the QD to C_{60} greatly enhances the ET process. This result rationalizes the experimental finding that mechanical mixtures[20] of CdSe QDs and C_{60} exhibit a notably poorer photoconversion performance than molecularly linked systems.[19] We have also shown that the ET process can be tuned by doping. The calculated ET times are in good agreement with the experimental data. The ET rate in the QD-C_{60} system interacting via a covalently bound bridge is enhanced due to the following three factors. (1) The bridge increases the nonadiabatic coupling by providing high-frequency vibrational modes and improving the donor−acceptor electronic interaction. (2) The bridge lowers the QD band gap and the average gap between the QD donor and C_{60} acceptor states because the QD wave functions extend onto the bridge, effectively increasing the QD size. (3) By providing long-range correlations between the atomic motions of the donor and acceptor species, the bridge decreases the phonon-induced pure-dephasing rate and prolongs quantum coherence during the nonadiabatic transition. The simulations indicate that the low-frequency polar vibrational modes of the CdSe QD as well as the vibrations of the bridging molecule promote the ET and accommodate the excess electronic energy. Our calculations clearly show that reliable covalent linking of the donor and acceptor species is extremely beneficial to efficient photoinduced charge separation in hybrid nanoscale materials. The reported time-domain ab initio simulations provide important insight into the fundamental chemical physics of the ET processes on the nanoscale and generate valuable guidelines for the improving performance of photovoltaic and photocatalytic devices.

AUTHOR INFORMATION

Corresponding Author

*E-mail: oleg.prezhdo@rochester.edu.

Notes

The authors declare no competing financial interest.

ACKNOWLEDGMENTS

Financial support of the CHE-1035196 grant of the National Science Foundation of the United States is gratefully acknowledged.

REFERENCES

(1) Mitchinson, A. Materials Science - Solar Cells Go Round the Bend. *Nature* **2008**, *455*, 744−744.
(2) Gratzel, M. Applied Physics - Solar Cells to Dye For. *Nature* **2003**, *421*, 586−587.
(3) Mallouk, T. E. Photoelectrochemistry - Bettering Natures Solar-Cells. *Nature* **1991**, *353*, 698−699.
(4) McGehee, M. D. Paradigm Shifts in Dye-Sensitized Solar Cells. *Science* **2011**, *334*, 607−608.
(5) Gur, I.; Fromer, N. A.; Geier, M. L.; Alivisatos, A. P. Air-Stable All-Inorganic Nanocrystal Solar Cells Processed from Solution. *Science* **2005**, *310*, 462−465; **2005**, *310*, 1618.
(6) Huynh, W. U.; Dittmer, J. J.; Alivisatos, A. P. Hybrid Nanorod-Polymer Solar Cells. *Science* **2002**, *295*, 2425−2427.
(7) Kamat, P. V.; Tvrdy, K.; Baker, D. R.; Radich, J. G. Beyond Photovoltaics: Semiconductor Nanoarchitectures for Liquid-Junction Solar Cells. *Chem. Rev.* **2010**, *110*, 6664−6688.
(8) Allen, C. G.; Baker, D. J.; Brenner, T. M.; Weigand, C. C.; Albin, J. M.; Steirer, K. X.; Olson, D. C.; Ladam, C.; Ginley, D. S.; Collins, R. T.; et al. Alkyl Surface Treatments of Planar Zinc Oxide in Hybrid Organic/Inorganic Solar Cells. *J. Phys. Chem. C* **2012**, *116*, 8872−8880.
(9) Dai, P. C.; Zhang, G.; Chen, Y. C.; Jiang, H. C.; Feng, Z. Y.; Lin, Z. J.; Zhan, J. H. Porous Copper Zinc Tin Sulfide Thin Film as Photocathode for Double Junction Photoelectrochemical Solar Cells. *Chem. Commun.* **2012**, *48*, 3006−3008.
(10) Nozik, A. J.; Beard, M. C.; Luther, J. M.; Law, M.; Ellingson, R. J.; Johnson, J. C. Semiconductor Quantum Dots and Quantum Dot Arrays and Applications of Multiple Exciton Generation to Third-Generation Photovoltaic Solar Cells. *Chem. Rev.* **2010**, *110*, 6873−6890.
(11) Zenkevich, E.; Cichos, F.; Shulga, A.; Petrov, E. P.; Blaudeck, T.; von Borczyskowski, C. Nanoassemblies Designed from Semiconductor Quantum Dots and Molecular Arrays. *J. Phys. Chem. B* **2005**, *109*, 8679−8692.
(12) Sambur, J. B.; Novet, T.; Parkinson, B. A. Multiple Exciton Collection in a Sensitized Photovoltaic System. *Science* **2010**, *330*, 63−66.
(13) Cheng, Y. J.; Cao, F. Y.; Lin, W. C.; Chen, C. H.; Hsieh, C. H. Self-Assembled and Cross-Linked Fullerene Interlayer on Titanium Oxide for Highly Efficient Inverted Polymer Solar Cells. *Chem. Mater.* **2011**, *23*, 1512−1518.
(14) Ju, T.; Graham, R. L.; Zhai, G. M.; Rodriguez, Y. W.; Breeze, A. J.; Yang, L. L.; Alers, G. B.; Carter, S. A. High Efficiency Mesoporous Titanium Oxide PbS Quantum Dot Solar Cells at Low Temperature. *Appl. Phys. Lett.* **2010**, *97*, 043106.
(15) Menzies, D. B.; Dai, Q.; Bourgeois, L.; Caruso, R. A.; Cheng, Y. B.; Simon, G. P.; Spiccia, L. Modification of Mesoporous TiO_2 Electrodes by Surface Treatment with Titanium(IV), Indium(III) and Zirconium(IV) Oxide Precursors: Preparation, Characterization and Photovoltaic Performance in Dye-Sensitized Nanocrystalline Solar Cells. *Nanotechnology* **2007**, 18.
(16) Duncan, W. R.; Prezhdo, O. V. Theoretical Studies of Photoinduced Electron Transfer in Dye-Sensitized TiO_2. *Annu. Rev. Phys. Chem.* **2007**, *58*, 143−184.
(17) Hayashi, H.; Lightcap, I. V.; Tsujimoto, M.; Takano, M.; Umeyama, T.; Kamat, P. V.; Imahori, H. Electron Transfer Cascade by Organic/Inorganic Ternary Composites of Porphyrin, Zinc Oxide Nanoparticles, and Reduced Graphene Oxide on a Tin Oxide

Electrode That Exhibits Efficient Photocurrent Generation. *J. Am. Chem. Soc.* **2011**, *133*, 7684−7687.
(18) Robel, I.; Bunker, B. A.; Kamat, P. V. Single-Walled Carbon Nanotube-CdS Nanocomposites as Light-Harvesting Assemblies: Photoinduced Charge-Transfer Interactions. *Adv. Mater.* **2005**, *17*, 2458−2463.
(19) Bang, J. H.; Kamat, P. V. CdSe Quantum Dot-Fullerene Hybrid Nanocomposite for Solar Energy Conversion: Electron Transfer and Photoelectrochemistry. *ACS Nano* **2011**, *5*, 9421−9427.
(20) Brown, P.; Kamat, P. V. Quantum Dot Solar Cells. Electrophoretic Deposition of CdSe−C_{60} Composite Films and Capture of Photogenerated Electrons with nC_{60} Cluster Shell. *J. Am. Chem. Soc.* **2008**, *130*, 8890−8891.
(21) Noone, K. M.; Subramaniyan, S.; Zhang, Q. F.; Cao, G. Z.; Jenekhe, S. A.; Ginger, D. S. Photoinduced Charge Transfer and Polaron Dynamics in Polymer and Hybrid Photovoltaic Thin Films: Organic vs Inorganic Acceptors. *J. Phys. Chem. C* **2011**, *115*, 24403−24410.
(22) Gocalinska, A.; Saba, M.; Quochi, F.; Marceddu, M.; Szendrei, K.; Gao, J.; Loi, M. A.; Yarema, M.; Seyrkammer, R.; Heiss, W.; et al. Size-Dependent Electron Transfer from Colloidal Pbs Nanocrystals to Fullerene. *J. Phys. Chem. Lett.* **2010**, *1*, 1149−1154.
(23) Song, N. H.; Zhu, H. M.; Jin, S. Y.; Zhan, W.; Lian, T. Q. Poisson-Distributed Electron-Transfer Dynamics from Single Quantum Dots to C60 Molecules. *ACS Nano* **2011**, *5*, 613−621.
(24) Shibu, E. S.; Sonoda, A.; Tao, Z. Q.; Feng, Q.; Furube, A.; Masuo, S.; Wang, L.; Tamai, N.; Ishikawa, M.; Biju, V. Photofabrication of Fullerene-Shelled Quantum Dots Supramolecular Nanoparticles for Solar Energy Harvesting. *ACS Nano* **2012**, *6*, 1601−1608.
(25) Chen, H. Y.; Lo, M. K. F.; Yang, G. W.; Monbouquette, H. G.; Yang, Y. Nanoparticle-Assisted High Photoconductive Gain in Composites of Polymer and Fullerene. *Nat. Nanotechnol.* **2008**, *3*, 543−547.
(26) Tully, J. C. Molecular Dynamics with Electronic Transitions. *J. Chem. Phys.* **1990**, *93*, 1061−1071.
(27) Craig, C. F.; Duncan, W. R.; Prezhdo, O. V. Trajectory Surface Hopping in the Time-Dependent Kohn-Sham Approach for Electron-Nuclear Dynamics. *Phys. Rev. Lett.* **2005**, *95*, 163001.
(28) Fischer, S. A.; Habenicht, B. F.; Madrid, A. B.; Duncan, W. R.; Prezhdo, O. V. Regarding the Validity of the Time-Dependent Kohn-Sham Approach for Electron-Nuclear Dynamics Via Trajectory Surface Hopping. *J. Chem. Phys.* **2011**, *134*, 024102.
(29) Habenicht, B. F.; Prezhdo, O. V. Nonradiative Quenching of Fluorescence in a Semiconducting Carbon Nanotube: A Time-Domain Ab Initio Study. *Phys. Rev. Lett.* **2008**, *100*, 197402.
(30) Habenicht, B. F.; Kalugin, O. N.; Prezhdo, O. V. Ab Initio Study of Phonon-Induced Denhasing of Electronic Excitations in Narrow Graphene Nanoribbons. *Nano Lett* **2008**, *8*, 2510−2516.
(31) Madrid, A. B.; Hyeon-Deuk, K.; Habenicht, B. F.; Prezhdo, O. V. Phonon-Induced Dephasing of Excitons in Semiconductor Quantum Dots: Multiple Exciton Generation, Fission, and Luminescence. *ACS Nano* **2009**, *3*, 2487−2494.
(32) Long, R.; Prezhdo, O. V. Ab Initio Nonadiabatic Molecular Dynamics of the Ultrafast Electron Injection from a PbSe Quantum Dot into the TiO_2 Surface. *J. Am. Chem. Soc.* **2011**, *133*, 19240−19249.
(33) Long, R.; English, N. J.; Prezhdo, O. V. Photo-Induced Charge Separation across the Graphene-TiO_2 Interface Is Faster Than Energy Losses: A Time-Domain Ab Initio Analysis. *J. Am. Chem. Soc.* **2012**, *134*, 14238−14248.
(34) Habenicht, B. F.; Prezhdo, O. V. Time-Domain Ab Initio Study of Nonradiative Decay in a Narrow Graphene Ribbon. *J. Phys. Chem. C* **2009**, *113*, 14067−14070.
(35) Kilina, S. V.; Kilin, D. S.; Prezhdo, V. V.; Prezhdo, O. V. Theoretical Study of Electron-Phonon Relaxation in PbSe and CdSe Quantum Dots: Evidence for Phonon Memory. *J. Phys. Chem. C* **2011**, *115*, 21641−21651.
(36) Neukirch, A. J.; Guo, Z. Y.; Prezhdo, O. V. Time-Domain Ab Initio Study of Phonon-Induced Relaxation of Plasmon Excitations in a Silver Quantum Dot. *J. Phys. Chem. C* **2012**, *116*, 15034−15040.
(37) Prezhdo, O. V.; Duncan, W. R.; Prezhdo, V. V. Photoinduced Electron Dynamics at the Chromophore-Semiconductor Interface: A Time-Domain Ab Initio Perspective. *Prog. Surf. Sci.* **2009**, *84*, 30−68.
(38) Perdew, J. P.; Burke, K.; Ernzerhof, M. Generalized Gradient Approximation Made Simple. *Phys. Rev. Lett.* **1996**, *77*, 3865−3868.
(39) Kresse, G.; Furthmuller, J. Efficiency of Ab-Initio Total Energy Calculations for Metals and Semiconductors Using a Plane-Wave Basis Set. *Comput. Mater. Sci.* **1996**, *6*, 15−50.
(40) Kresse, G.; Joubert, D. From Ultrasoft Pseudopotentials to the Projector Augmented-Wave Method. *Phys. Rev. B* **1999**, *59*, 1758−1775.
(41) Feng, M.; Zhao, J.; Petek, H. Atomlike, Hollow-Core-Bound Molecular Orbitals of C60. *Science* **2008**, *320*, 359−362.
(42) Weaver, J. H.; Martins, J. L.; Komeda, T.; Chen, Y.; Ohno, T. R.; Kroll, G. H.; Troullier, N.; Haufler, R. E.; Smalley, R. E. Electronic-Structure of Solid C60 - Experiment and Theory. *Phys. Rev. Lett.* **1991**, *66*, 1741−1744.
(43) Tvrdy, K.; Frantsuzov, P. A.; Kamat, P. V. Photoinduced Electron Transfer from Semiconductor Quantum Dots to Metal Oxide Nanoparticles. *Proc. Natl. Acad. Sci. U.S.A.* **2011**, *108*, 29−34.
(44) Kilina, S.; Ramirez, J.; Tretiak, S. Brightening of the Lowest Exciton in Carbon Nanotubes Via Chemical Functionalization. *Nano Lett* **2012**, *12*, 2306−2312.
(45) Fernandez-Alberti, S.; Roitberg, A. E.; Nelson, T.; Tretiak, S. Identification of Unavoided Crossings in Nonadiabatic Photoexcited Dynamics Involving Multiple Electronic States in Polyatomic Conjugated Molecules. *J. Chem. Phys.* **2012**, *137*, 014512.
(46) Prezhdo, O. V. Quantum Anti-Zeno Acceleration of a Chemical Reaction. *Phys. Rev. Lett.* **2000**, *85*, 4413−4417.